# A non-selenization technology by co-sputtering deposition for solar cell applications

**Bao-Tang Jheng,[1] Po-Tsun Liu,[2,*] Meng-Chyi Wu,[1] and Han-Ping D. Shieh[2]**

[1]*Department of Electrical Engineering, National Tsing Hua University, Hsinchu City, Taiwan*

[2]*Department of Photonics & Display Institute, National Chiao Tung University, Hsinchu City, Taiwan*

**Corresponding author: ptliu@mail.nctu.edu.tw*

Received February 13, 2012; revised March 22, 2012; accepted March 22, 2012;
posted March 30, 2012 (Doc. ID 162757); published June 29, 2012

This work presents a novel method to form polycrystalline $Cu(In_{1-x}Ga_x)Se_2$ (CIGS) thin film by co-sputtering of In—Se and Cu—Ga alloy targets without an additional selenization process. An attempt was also made to thoroughly elucidate the surface morphology, crystalline phases, physical properties, and chemical properties of the CIGS films by using material analysis methods. Experimental results indicate that CIGS thin films featured densely packed grains and chalcopyrite phase peaks of (112), (220), (204), (312), and (116). Raman spectroscopy analysis revealed chalcopyrite CIGS phase with Raman shift at 175 $cm^{-1}$, while no signal at 258 $cm^{-1}$ indicated the exclusion of $Cu_{2-x}Se$ phase. Hall effect measurements confirmed the polycrystalline $Cu(In, Ga)Se_2$ thin film to be of $p$ type semiconductor with a film resistivity and mobility of $2.19 \times 10^2$ Ω cm and 88 $cm^2/V s$, respectively. 

*OCIS codes:* 350.0350, 350.6050.

Polycrystalline $Cu(In, Ga)Se_2$ (CIGS)-based solar cell has emerged as one of the most promising absorber materials for inexpensive, high-efficiency solar cell applications, because of its tunable bandgap ($1.04 \sim 1.68$ eV), high-absorption coefficient ($\alpha > 10^5$ $cm^{-1}$), high-tolerance to defects and impurities, as well as the highest conversion efficiencies of approximately 20% efficiency in the laboratory [1]. Among the various CIGS manufacturing processes include co-evaporation [2], selenization [3], sputtering [4] and electrode position [5]. However, the co-evaporation process, by which the record efficiency cell was achieved, is generally considered to be insufficient for mass production, because of its procedural complexity and difficulties in scaling up for a large manufacturing system. However, a two-step process, in which the postselenization step follows the sputtering step of the metallic precursors, is easier to scale up and appears to be the most feasible approach for industrial production. Metallic precursors have been selenized using many postselenization approaches [6,7].

Selenization of metal layers using $H_2Se$ gas or Se-vapor from a solid source allows the CIGS-based solar cell with a sunlight to electricity to achieve a conversion efficiency of 16.2% and 10.2%, respectively [8,9]. However, most of these two-stage metallic precursors have certain limitations, including the use of highly toxic $H_2Se$, and poor adhesion to the interface between Mo and CIS due to large volume expansion stresses originating from the selenization process [10]. Developing a nonselenization process is thereby important, especially when considering environmental protection and promoting film adhesion. Magnetron co-sputtering is a conventional deposition process to form CIGS films because it is a simple and mature approach, capable of providing excellent uniformity over large areas with a high deposition rate.This work develops a chalcopyrite CIGS thin film without an additional selenization process by using magnetron co-sputtering from the targets of Cu—Ga and In—Se alloys. Capable of eliminating a complex postselenization process with various chemical precursors, the proposed CIGS film is simple, inexpensive and promising for use in large-area production technology for solar cell applications. Finally, the optimum film characteristics are investigated based on the structural, compositional, electrical, and optical properties of films.

A CIGS film with an area of 5 cm × 5 cmwas deposited using an inline sputtering system, consisting of a two-gun sputtering chamber and a heating chamber connected by a loadlock chamber. DC/RF powers were supplied by DC/RF generators from Advanced Energy. Additionally, a base pressure of $5 \times 10^{-7}$ Torr in the sputtering chamber and $2 \times 10^{-6}$ Torr in annealing chamber was pumped down by a cryogenic pump and diffusion pump, respectively. Sputtering parameters for the deposition of CIGS films were as follows: room temperature, working Ar gas pressure of 0.75–0.93 Pa, RF sputtering power of 80–150 W, DC sputtering power of 20 W, and argon gas flow rate of 30–70 SCCM. The $Cu(In, Ga)Se_2$ films were deposited on soda-lime glass substrates via co-sputtering of Cu—Ga alloy, In—Se alloy targets. The annealed temperature is divided into two steps. In the first step, the furnace temperature was maintained at 350 °C for 15 min to form the chalcopyrite phase. Second, the furnace temperature was increased to 580 °C for 10 min to achieve recrystallization and grain growth.

Figures 1(a)–1(c) show the surface morphologies of the as-deposited CIGS films at different working pressures. The working pressures ranged from 8 to 12 mTorr. Also, the morphology of CIGS films was smooth and dense. According to these figures, crystallinity of the films improved when decreasing the working pressures; and the film became compact. Additionally, the surface roughness increased as the grain size enlarged with an

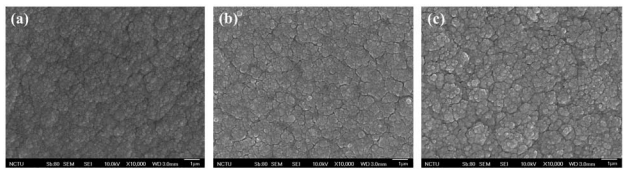


Fig. 1. SEM images of the CIGS films as-deposited with different working pressures: (a) 8 mTorr, (b) 10 mTorr; (c) 12 mTorr.

 

**Table 1. Sputtering Parameters and Hall Measurement Results of the Annealed CIGS Films Prepared with Different Working Pressures**

| Sample | Pressure [mTorr] | Thickness [nm] | Concentration [$cm^{-3}$] | Mobility [$cm^2/V\,s$] | Resistivity [Ω-cm] | Adhesion [fail/pass] |
|---|---|---|---|---|---|---|
| 1 | 8 | 1539 | $3.24 \times 10^{16}$ | 88 | $2.19 \times 10^2$ | Pass |
| 2 | 10 | 1537 | $6.47 \times 10^{14}$ | 43 | $2.21 \times 10^2$ | Pass |
| 3 | 12 | 1534 | $9.07 \times 10^{14}$ | 30 | $2.24 \times 10^2$ | Pass |

increasing working pressure. The kinetic energy of CIGS ions decreased due to increased particle scattering, while the working pressure increased. Consequently, the film became less dense with a significant amount of region boundaries. Also, the film could not crystallize well

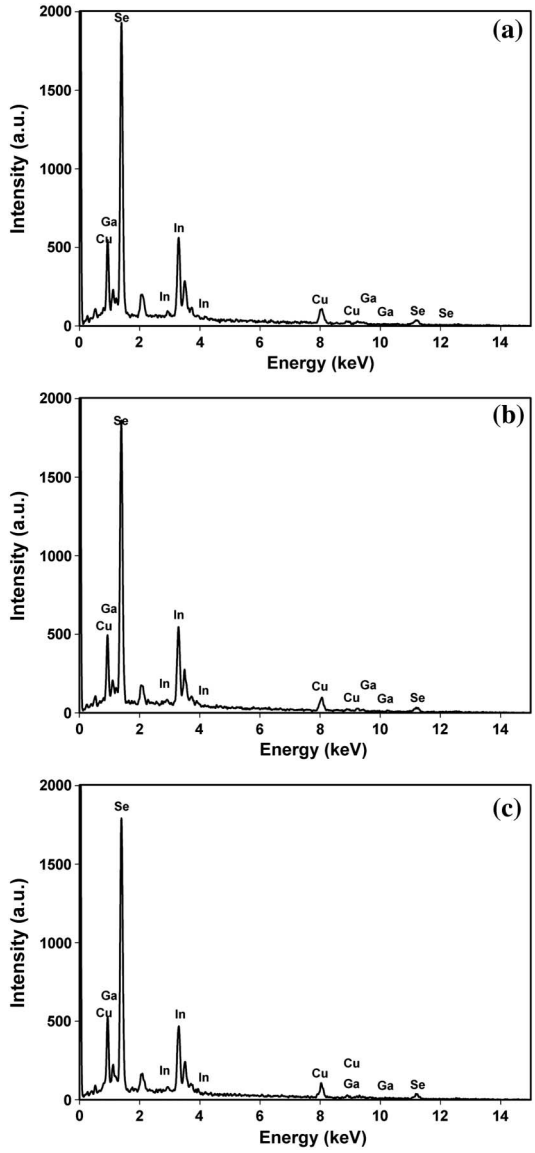


Fig. 2. Energy dispersive spectrometer (EDS) composition analysis of annealed CIGS films with different working pressures: (a) 8 mTorr, (b) 10 mTorr; (c) 12 mTorr.

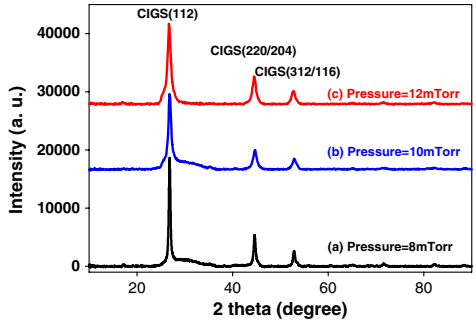


Fig. 3. (Color online) XRD patterns of the annealed CuInGaSe precursor films deposited at various working pressure (a) 8 mTorr, (b) 10 mTorr; (c) 12 mTorr.

resulting in a slight increase of the film resistivity. Adhesion tests were also performed using a Kapton tape for the CIGS films listed in Table 1, indicating that the CIGS films have good adhesion.

Figures 2(a)–2(c) show the energy dispersive X-ray spectroscopy analyses of the $CuInGaSe_2$ films. Contents of the selenium element were sufficiently observed in all $CuInGaSe_2$ films without additional selenization treatment. The high content of Se incorporation is necessary to ensure CIGS films exhibiting strong $p$ type semiconductors Additionally, the $Cu:(In + Ga):Se$ atomic ratios of $1:1:2$ were observed in all CIGS thin films. The stoichiometry ratios of the CIGS film were $Cu/(In + Ga) = 0.85$ and $Ga/(In + Ga) = 0.23$, which approached to the device-quality stoichiometry ratio ($Cu/(In + Ga) < 0.90$, and $Ga/(In + Ga) < 0.3$).

Figures 3(a)–3(c) show the x-ray diffraction (XRD) of the thermally annealed CuInGaSe films, prepared at different working pressures. All CIGS thin films show the peaks corresponding to the chalcopyrite-type CIGS structure.

XRD spectra contained several obvious peaks appearing near the locations of the signal peaks (112), (220), (204), (312) and (116), respectively. All CIGS films have the properties of chalcopyrite crystal compounds with narrow crystalline peaks. Our results further confirmed a large crystal structure with a similar XRD pattern and the sharpest diffraction peak (112). Additionally, a single-phase $Cu_1In_{0.7}Ga_{0.3}Se_2$ was only detected. Above observations reveal that CIGS films with (112/220/204)-oriented densely packed grains can reduce carrier recombination and the leakage current having originated from the structural defects in the thin film. This reduction can improve

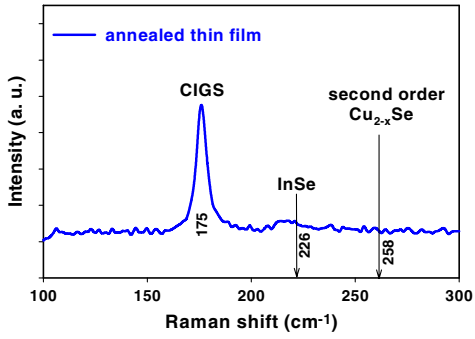


Fig. 4. (Color online) Raman scans of two-stage annealed CIGS thin films for working pressures of 8 mTorr.

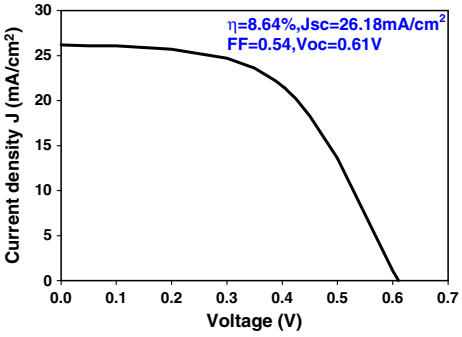


Fig. 5. (Color online) Photocurrent voltage ($I$-$V$) characteristic of the fabricated CIGS solar cell.

the electrical features of the CIGS solar cell, such as an open circuit voltage ($V_{oc}$) and short circuit current density ($J_{sc}$) [11]. Furthermore, intensity of the main (112) peak decreased with an increasing working pressure, and its FWHM widened as well. This finding suggests that the crystallinity of CIGS film degrades with an increasing working pressure because the free radicals of reactants have a higher kinetic energy under a lower working pressure. Thus, the CIGS polycrystalline can be rebuilt layer by layer on the substrate.

Figure 4 shows the micro-Raman spectrum of annealed CIGS absorber films. The major peak appearing at 175 $cm^{-1}$ denotes the CIGS phase. The peak appearing at 258 $cm^{-1}$ is commonly attributed to binary copper selenides compound ($Cu_{2-x}Se$) [12]; in addition, the peak appearing at 226 $cm^{-1}$ exhibits the presence of InSe [13]. A Raman shift at 175 $cm^{-1}$ (Fig. 4) was attributed to the formation of quaternary chalcopyrite (CH) CIGS phase, while no Raman signal at 258 $cm^{-1}$ referred to the exclusion of second order $Cu_{2-x}Se$ phase [14]. Similar results were obtained in Samples 1 and 2. This finding suggests that thermal annealing reduces the defects amounts and extra binary phases. This reduction can lead to homogeneous optoelectronic properties and a low density of recombination centers, further improving solar cell efficiency [15].

This work also examined the quality of the nonselenized CIGS layers for CIGS solar cell applications, glass/Mo/CIGS/CdS/intrinsic-ZnO/ZnO:Al/Al grids, were also fabricated. An approximately 50 nm thick CdS buffer layer was deposited by chemical bath deposition (CBD) using $CdSO_4$ (0.15 M)—ammonia (7.4 M)—thiourea (0.5 M) aqueous solutions at 85 °C. A layer of 50 nm thick intrinsic ZnO and 500 nm thick ZnO:Al (2wt% $Al_2O_3$-doped ZnO) thin films was then deposited at room temperature by RF sputtering. Figure 5 shows the photocurrent voltage ($I$-$V$) curve of the fabricated CIGS cell. Efficiencies as high as 8–9% were achieved for the manufactured CIGS solar cells without additional selenization. Figure 6 shows 86% external quantum efficiency (EQE) for the CIGS solar cell. This figure reveals that the MO/CIGS/CdS device exhibited excellent quantum efficiency for the incident solar light with wavelengths ranging from 500 to 800 nm.

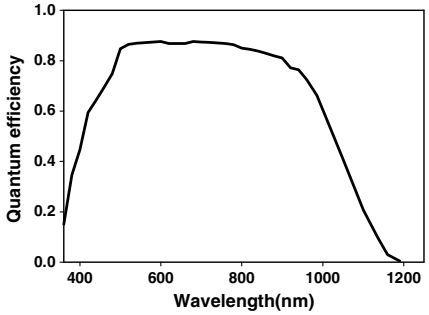


Fig. 6. External quantum efficiency of the CIGS solar cell.

In summary, this work achieved growth of CIGS thin films by using a simple co-sputtering process. A sufficient content of Se can be incorporated into the Cu(In, Ga)$Se_2$ films without the need for additional selenium source in vacuum. Additionally, the annealed CIGS films have large grain sizes, smooth surfaces, and shortage of Cu—Se second-phase. According to XRD analysis results, the single-phase chalcopyrite structure with preferential orientation of (112) direction is indicative of adequate elemental mixing. Moreover, Hall measurements confirmed that the annealed thin film has $p$ type semiconductor characteristics, and the carrier concentration, dark resistivity, and Hall mobility are $3.24 \times 10^{16}$ $cm^{-3}$, $2.19 \times 10^2$ Ω cm and 88 $cm^2/V\,s$, respectively. Furthermore, the CIGS solar cells exhibited an efficiency as high as 8–9%. Our results demonstrate that the proposed thin film co-sputtering method can produce high quality Cu(In, Ga)$Se_2$ films for photovoltaic applications.

This work was partially performed at Laboratory for Roll to Roll Plasma Coating Technology in Institute of Nuclear Energy Research under grant NSC1002001I-NER038, Taiwan.

## References

1. I. Repins, M. A. Contreras, B. Egaas, C. DeHart, J. Scharf, C. Perkins, B. To, and R. Noufi, Prog. Photovoltaics **16**, 235 (2008).
2. A. M. Gabor, J. R. Tuttle, D. S. Albin, M. A. Contreras, and R. Noufi, Appl. Phys. Lett. **65** 198 (1994).
3. M. Kaelin, D. Rudmanna, F. Kurdesaua, T. Meyer, H. Zogga, and A. N. Tiwari, Thin Solid Films **431** 58 (2003).
4. D. G. Moon, S. Ahn, J. H. Yun, A. Cho, J. Gwak, S. Ahn, K. Shin, K. Yoon, H. D. Lee, H. Pak, and S. Kwon, Sol. Energy Mater. Sol. Cells **95** 2786 (2011).
5. A. M. Fernandez and R. N. Bhattacharya, Thin Solid Films **474** 10 (2005).
6. C. Y. Su, W. H. Ho, H. C. Lin, C. Y. Nieh, and S. C. Liang, Sol. Energy Mater. Sol. Cells **95**, 261 (2011).
7. J. C. Chang, C. C. Chuang, J. W. Guo, S. C. Hsu, H. R. Hsu, C. S. Wu, and T. P. Hsieh, Nanosc. Nanotechnol. Lett. **3**, 200 (2011).
8. R. Gay, in *Proceedings of the 12th European Photovoltaic Solar Energy Conference* (1994), p. 935.
9. F. B. Dejene, Sol. Energy Mater. Sol. Cells **93**, 577 (2009).
10. Y. E. Lee, H. J. Kim, Y. J. Kim, K. K. Lee, and B. H. Choi, J. Electrochem. Soc. **141**, 558 (1994).
11. A. M. Hermann and C. Gonzalez, Sol. Energy Mater. Sol. Cells **70**, 345 (2001).
12. M. Grossberg and L. Kaupmees, Sol. Energy Mater. Sol. Cells **93**, 11 (2009).
13. O. A. Balitskii and V. P. Savchyn, Semicond. Sci. Technol. **17**, L1 (2002).
14. W. Witte, R. Kniese, M. Powalla, W. Witte, R. Kniese, and M. Powalla, Thin Solid Films **517**, 867 (2008).
15. M. A. Contreras, M. J. Romero, and R. Noufi, Thin Solid Films **511**, 51 (2006).